Crystal structure of a Signal Recognition Particle *Alu* domain in the elongation arrest conformation

Luc Bousset[1,3], Camille Mary[2,4], Mark A. Brooks[1,5], Anne Scherrer[2], Katharina Strub[2] and Stephen Cusack[1]*

Supplementary Material

Supplementary (Online) Methods

Reconstitution of *PhAlu* RNA complexes with hSRP9/14

Human SRP9 residues 1 to 85 and SRP14 residues 1 to 107 proteins were expressed in *Escherichia coli* BL21(DE3) using pET vectors, as described previously(Bovia et al. 1997). Selenomethionine (Se-Met) labeled SRP9 and SRP14 were produced in the same strain, under modified growth conditions(Van Duyne et al. 1993). SRP9 and SRP14 were purified separately on Heparin Sepharose (GE Healthcare) and Bio-S ion exchange columns, respectively (Bio-Rad), followed by reconstitution of the heterodimer in solution at an equi-molar ratio. The SRP9/14 complex further purified using a Bio-S column followed by size exclusion chromatography (Superdex 200, GE Healthcare). *P. horikoshii* SRP *Alu* DNA coding sequences were obtained by gene synthesis(Hoover and Lubkowski 2002). GUAA tetraloops were inserted to replace the SRP RNA S-domain, together with a 3´ hammerhead ribozyme. PCR fragments were cloned into pSP64 vector and the DNAs of each of the plasmids were fully sequenced. Amplified vectors were linearised with *Hind* III. *Alu* RNAs were transcribed *in vitro* and gel purified as described previously(Price et al. 1995) and refolded prior to complex formation by annealing at 65°C followed by a slow cooling step. Complex formation with SRP9/14 proceeded at 37°C for 10 minutes with a 30% excess of protein. RNPs were then purified on a Superdex 200 gel filtration column, concentrated up to 5 mg/ml and then stored at 4°C.

Crystallization and data collection

Crystals of selenomethionine-labeled and native SRP9/14–RNA complex were grown in hanging drops formed by a 1:1 mixture of the complex at 5 mg/ml and

crystallization buffer. *PhAlu*134 complex crystals grew in a crystallization solution containing 17.5% PEG 400, 5% glycerol buffered in 100 mM sodium acetate pH 5.0. Crystals grew at 4°C in three days and belong to the space group $P4_32_12$ (a=b=100.45Å, c=196.71 Å, α=β=γ=90°). Crystals of the *PhAlu*110 complex were obtained with a crystallization solution containing 17.5% PEG 3350, 2.5% glycerol, 0.3 M ammonium sulphate and 0.1 M sodium acetate at pH 4.6. Crystals grew at 4°C in 24 hours and belong to the orthorhombic space group $P2_12_12_1$ (a=104.13 Å, b=108.8 Å, c=128.26 Å, α=β=γ=90°).

Cryoprotection was achieved by adding 20% glycerol before freezing at 100K. A *PhAlu*134 crystal diffracting to 3.6Å resolution on ESRF beamline BM30A allowed collection of a three-wavelength MAD dataset. A higher resolution dataset to 3.2 Å was subsequently collected on the ESRF beamline ID14-1. *PhAlu*110 crystals diffracted X-rays to 3.35 Å on ESRF beamline ID23-1. Diffraction data were processed using XDS(Kabsch 1993). Data collection statistics are summarized in Supplementary Table 1.

Phasing and refinement

Six of the seven selenium atoms of the *PhAlu*134 complex were located from the MAD data using reflections to 4.5 Å resolution with SOLVE(Terwilliger and Berendzen 1999) and the final figure of merit of the experimental phases was 0.53. Phases were improved by solvent flattening using SOLOMON and DM(Cowtan 1993) as implemented in SHARP with a 60% solvent content. The electron density map was of sufficient quality (Supplementary Figure 2) for a modeling and refinement to proceed using COOT(Emsley and Cowtan 2004) and REFMAC, resulting in an atomic model with an R_{work}/R_{free} of 0.193/0.228. The RNA geometry was significantly improved with

PHENIX-ERRASER (https://www.phenix-online.org/documentation/erraser.htm). The structure of the *PhAlu*110 complex was solved by molecular replacement using Phaser(McCoy et al. 2007) with the *PhAlu*134 structure as model and refined to an R_{work}/R_{free} of 0.192/0.237. For both structrues, map quality was considerably enhanced using map sharpening as implemented in REFMAC. The structure of SRP9/14 is relatively unchanged compared to that found in previous complexes lacking RNA stem 5 (RMSD of 0.9 Å over 147 SRP9/14 Cα positions, compared to the model with PDB accession code 1E8O(Weichenrieder et al. 2000)). Nevertheless, certain residues that were disordered in previous structures of SRP9/14 were found to be traceable in the electron density, including half of the large internal loop of SRP14. Figures were prepared using PYMOL(DeLano 2002) and MOLSCRIPT(Kraulis 1991) and BOBSCRIPT(Esnouf 1997).

Elongation arrest and translocation activities

7SLC reconstitutes more efficiently into SRP than the previously used construct and exhibited similar activity in elongation arrest activity (Lakkaraju et al. 2008; Mary et al. 2010). 7SLC RNAs were expressed as described previously (Huck et al. 2004). After purification on G50 columns, the RNAs were extracted 2x with phenol/dichloromethane and 2x with dichloromethane and lyophilized. The RNA concentrations were determined by OD_{260} and compared by denaturing gel electrophoresis. Native gels were performed as described (Huck et al. 2004). Particles were assembled at 0.5 µM of recombinant human SRP19, recombinant canine SRP54 and canine SRP68/72 and at 2 µM synthetic RNAs (7SLC or PAHS). Concentration of SRP9/14 was 4uM. The excess of PAHS RNA, and as a control also of 7SLC RNA, is required for maximal yield of functional particles,

since not all of the synthetic RNA is in its native structure. For protein purifications and elongation arrest and translocation assays see Huck *et al.,* 2004. Briefly, the final concentration of SRP in the wheat germ translation reactions was 100 nM based on the SRP54 concentration. . For the processing assay EDTA and salt-washed membranes (EKRM) were added to translation reactions at final concentrations of 0.02 eq/μL, respectively, as described (Thomas et al. 1997). For elongation arrest and translocation assays, the reactions were stopped at 20 min. and 35 min., respectively. The *in vitro* synthesized proteins were quantified by phosphorescence imaging. The relative inhibition of preprolactin accumulation was calculated as follows: $\text{Inhibition}[\%]=\left[1-\left(\frac{P_s}{C_s}\Big/\frac{P_o}{C_o}\right)\right]*100$. P_s and C_s are the amounts of preprolactin and cyclin quantified in the sample and P_o and C_o the amounts present in the negative control (buffer). The translocation efficiency was calculated as follows: $T = 100^* PL/(PL + pPL)$, where PL is prolactin and pPL preprolactin.

RNA transcript sequences

The 'PAHS' RNA used in the translocation assays consisted of stems 1, 2, 3 & 4 of archaeal SRP RNA fused to the complementary stems of human SRP RNA, and was of the following sequence:

GGGGCTAGGCCGGGGGGTTCGGCGTCCCCTGTAACCGGAAACCGCCGATATGCCGGGGCCGAAGA
GGTGGGAGGATCGCTTGAGCCCAGGAGTTCTGGGCTGCAGTGCGCTATGCCGATCGGGTGTCCGC
ACTAAGTTCGGCATCAATATGGTGACCTCCCGGGAGCGGGGGACCACCAGGTTGCCTAAGGAGGG
GTGAACCGGCCCAGGTCGGAAACGGAGCAGGTCAAAACTCCCGTGCTGATCAGTAGTGGGATCGC
GCCTGTGAATAGCCACTGCACTCCAGCCTGGGCAACATAGCGAGACCCCGTGTCGTGCCCCAAGC
TT

The ‘7SLC’ RNA represents a circular permutation of 7SL RNA (5′ and 3′ ends at positions 280 and 277 in 7SL RNA, respectively). The sequence of 7SLC transcribed in the translocation assays was as follows:

GATAGCGAGACCCCGCCTCTTTTGCCGGGCGCGGTGGCGCGCGCCTGTAGTCCCAGCTACTCGGG
AGGCTGAGGCGGGAGGATCGCTTCTGCCCAGGAGTTCTGGGCTGCAGTGCGCTATGCCGATCGGG
TGTCCGCACTAAGTTCGGCATCAATATGGTGACCTCCCGGGAGCGGGGGACCACCAGGTTGCCTA
AGGAGGGGTGAACCGGCCCAGGTCGGAAACGGAGCAGGTCAAAACTCCCGTGCTGATCAGTAGTG
GGATCGCGCCTGTGAATAGCCACTGCACTCCAGCCTGGGCTTT

Supplementary Tables

Supplementary Table 1. Data collection statistics.

§ $R_{sym} = \Sigma_{hkl} \Sigma_i | \langle I \rangle_{hkl} - I_{hkl,i}| / \Sigma_{hkl} \Sigma_i I_{hkl,i}$, where $\langle I \rangle_{hkl}$ is the mean intensity and $I_{hkl,i}$ is the intensity of the ith measurement of reflection I_{hkl}. †Values in parentheses refer to the highest resolution shells. *Friedel pairs were treated as separate reflections.

hSRP9/14 with		***PhAlu*134**			***PhAlu*110**
Identifier	Peak*	Inflection*	Remote I*	Remote II*	Native
	BM30A	BM30A	BM30A	ID14-EH1	ID23-EH1
Wavelength (Å)	0.9808	0.9809	0.9763	0.934	0.979
Space group		$P4_32_12$			$P2_12_12_1$
Unit cell parameters (Å)		*a*=100.5, *b*=100.5, *c*=196.9 α=β=ɣ=90°		*a*=100.9, *b*=100.9, *c*=197.5 α=β=ɣ=90°	*a*=104.1, *b*=108.8, *c*=128.3 α=β=ɣ=90°
Resolution (Å) (outer shell limits)	50 - 3.6 (3.7-3.6)	50 - 3.6 (3.7-3.6)	50 - 3.6 (3.7-3.6)	30 – 3.2 (3.4-3.2)	30-3.4 (3.5-3.4)
R_{sym} (%)§	11.1 (54.3)	10.1 (49.7)	13.0 (65.8)	7.6 (63.7)	9.9 (71.0)
⟨I⟩/⟨σ(I)⟩†	11.7 (3.22)	11.8 (3.10)	9.63 (2.35)	9.09 (1.74)	9.45 (2.04)
Reflections measured†	94090 (6548)	85762 (6053)	85617 (5866)	67089 (10569)	82812 (6859)
Unique reflections measured†	21989 (1587)	22024 (1601)	22059 (1575)	30821 (4846)	20536 (1685)
Completeness (%)	99.5 (97.2)	99.4 (98.8)	99.5 (96.4)	97.8 (95.9)	99.5 (99.9)

Supplementary Table 2. Refinement statistics.

Complex	***PhAlu*134**	***PhAlu*110**
Resolution (Å)	89.2 – 3.22	80.73 – 3.35
No. reflections	16238	20150
R_{work} (last shell)	0.193 (0.342)	0.192 (0.363)
R_{free} (last shell)	0.228 (0.424)	0.237 (0.333)
No. atoms	4261	7248
Protein	1379	2526
RNA	2882	4722
***B*-factors**	130.3	118.9
Protein	122.0	125.2
RNA	134.0	116.0
R.M.S. deviations		
Bond lengths (Å)	0.005	0.004
Bond angles (°)	1.08	0.948
Ramachandran plot		
Favoured (%)	91.6	88.8
Outliers (%)	0.0	0.0

Supplementary Table 3: Quantitation of elongation arrest and translocation assays

Inhibition [%]			**Translocation [%]**		
RC 7SLC	Mean	SEM	RC 7SLC	Mean	SEM
WT	71	4	WT	73	4
A12	22	2	A12	35	7
100	85	11	100	78	2
(-9/14)	26	5	(-9/14)	21	3

Inhibition [%]			**Translocation [%]**		
RC PAHS	Mean	SEM	RC PAHS	Mean	SEM
WT	76	5	WT	68	6
A12	30	7	A12	38	7
100	98	11	100	75	1
(-9/14)	28	3	(-9/14)	22	4

Supplementary References

Bovia F, Wolff N, Ryser S, Strub K. 1997. The SRP9/14 subunit of the human signal recognition particle binds to a variety of Alu-like RNAs and with higher affinity than its mouse homolog. *Nucleic acids research* **25**: 318-326.

Bricogne G, Vonrhein C, Flensburg C, Schiltz M, Paciorek W. 2003. Generation, representation and flow of phase information in structure determination: recent developments in and around SHARP 2.0. *Acta crystallographica* **59**: 2023-2030.

Cowtan KD. 1993. Improvement of macromolecular electron-density maps by the simultaneous application of real and reciprocal space constraints. *Acta crystallographica Section D, Biological crystallography* **49**: 148-157.

DeLano W. 2002. The PyMOL Molecular Graphics System. DeLano Scientific, San Carlos, CA, USA.

Emsley P, Cowtan K. 2004. Coot: model-building tools for molecular graphics. *Acta crystallographica* **60**: 2126-2132.

Esnouf RM. 1997. An extensively modified version of MolScript that includes greatly enhanced coloring capabilities. *J Mol Graph Model* **15**: 132-134, 112-133.

Halic M, Becker T, Pool MR, Spahn CM, Grassucci RA, Frank J, Beckmann R. 2004. Structure of the signal recognition particle interacting with the elongation-arrested ribosome. *Nature* **427**: 808-814.

Hoover DM, Lubkowski J. 2002. DNAWorks: an automated method for designing oligonucleotides for PCR-based gene synthesis. *Nucleic acids research* **30**: e43.

Huck L, Scherrer A, Terzi L, Johnson AE, Bernstein HD, Cusack S, Weichenrieder O, Strub K. 2004. Conserved tertiary base pairing ensures proper RNA folding and efficient assembly of the signal recognition particle Alu domain. *Nucleic acids research* **32**: 4915-4924.

Kabsch W. 1993. Automatic processing of rotation diffraction data from crystals of initially unknown symmetry and cell constants. *Journal of Applied Crystallography* **26**: 795-800.

Kraulis PJ. 1991. MOLSCRIPT: A Program to Produce Both Detailed and Schematic Plots of Protein Structures. *Journal of Applied Crystallography* **24**: 946-950.

Lakkaraju AK, Mary C, Scherrer A, Johnson AE, Strub K. 2008. SRP keeps polypeptides translocation-competent by slowing translation to match limiting ER-targeting sites. *Cell* **133**: 440-451.

Mary C, Scherrer A, Huck L, Lakkaraju AK, Thomas Y, Johnson AE, Strub K. 2010. Residues in SRP9/14 essential for elongation arrest activity of the signal recognition particle define a positively charged functional domain on one side of the protein. *Rna* **16**: 969-979.

McCoy AJ, Grosse-Kunstleve RW, Adams PD, Winn MD, Storoni LC, Read RJ. 2007. Phaser crystallographic software. *J Appl Crystallogr* **40**: 658-674.

Price SR, Ito N, Oubridge C, Avis JM, Nagai K. 1995. Crystallization of RNA-protein complexes. I. Methods for the large-scale preparation of RNA suitable for crystallographic studies. *J Mol Biol* **249**: 398-408.

Terwilliger TC, Berendzen J. 1999. Automated MAD and MIR structure solution. *Acta crystallographica Section D, Biological crystallography* **55 (Pt 4)**: 849-861.

Thomas Y, Bui N, Strub K. 1997. A truncation in the 14 kDa protein of the signal recognition particle leads to tertiary structure changes in the RNA and abolishes the elongation arrest activity of the particle. *Nucleic acids research* **25**: 1920-1929.

Van Duyne GD, Standaert RF, Karplus PA, Schreiber SL, Clardy J. 1993. Atomic structures of the human immunophilin FKBP-12 complexes with FK506 and rapamycin. *J Mol Biol* **229**: 105-124.

Weichenrieder O, Wild K, Strub K, Cusack S. 2000. Structure and assembly of the Alu domain of the mammalian signal recognition particle. *Nature* **408**: 167-173.

Supplementary Figure Legends

Supplementary Figure 1

Characterization of *PhAlu* RNA : SRP9/14 complexes by size exclusion chromatography using a Superdex200-16/60 column (GE Healthcare) equilibrated in a buffer containing 20 mM Hepes pH 7.5, 150 mM NaCl and 5 mM $MgCl_2$.

(A) Elution profile of *PhAlu*134 RNA alone (dashed line) and *PhAlu*134 RNA:SRP9/14 complex (solid line).

(B) Elution profile of *PhAlu*110 RNA alone (dashed line) and *PhAlu*110 RNA:SRP9/14 complex (solid line).

(C) SDS-PAGE analysis of purified *PhAlu*134:SRP9/14 complex revealed by silver staining.

(D) SDS-PAGE analysis of purified *PhAlu*110 RNA:SRP9/14 complex revealed by Coomassie blue (left panel) and urea-PAGE gel stained with methylene blue.

Supplementary Figure 2

Stereo view of the experimental electron density map of *PhAlu*134 RNA superposed with the final model (yellow backbone, red bases), contoured at 0.8 sigma calculated from MAD data after heavy atom substructure refinement, phase calculation and solvent flattening with SHARP (Bricogne et al. 2003).

Supplementary Figure 3

(A) Superposition of *PhAlu*134 (red) and *PhAlu*110 (green) RNAs showing very high structural similarity except in the distal 5′ stem region. *PhAlu*134 shows a bend in the region assigned to hinge 2 in the cryo EM map of the complete mammalian SRP bound to the ribosome (Halic et al. 2004).

(B) Schematic depiction of the secondary structure of the *PhAlu*134 (green and red nucleotides) and *PhAlu*110 (green only) RNAs.

Supplementary Figure 4

(A) Secondary structure of PAHS RNA.

(B) and (C) Elongation arrest and translocation activities of SRPs. [^{35}S]-labeled translation products displayed by SDS-PAGE. SRP was reconstituted with either 7SLC or PAHS RNA together with recombinant (SRP19, SRP54) and canine (SRP68/72) proteins as well as the SRP9/14 proteins indicated. WT: SRP9/14; -9/14: without SRP9/14; A12: SRP9/14A12; -100: SRP9/14-100. Cyc: Truncated version of cyclin; pPL: Preprolactin; PL: Prolactin. Final SRP concentration in the translation reaction: 100 nM, EKRM: 0.02 eq./µl.

Supplementary Figure 1

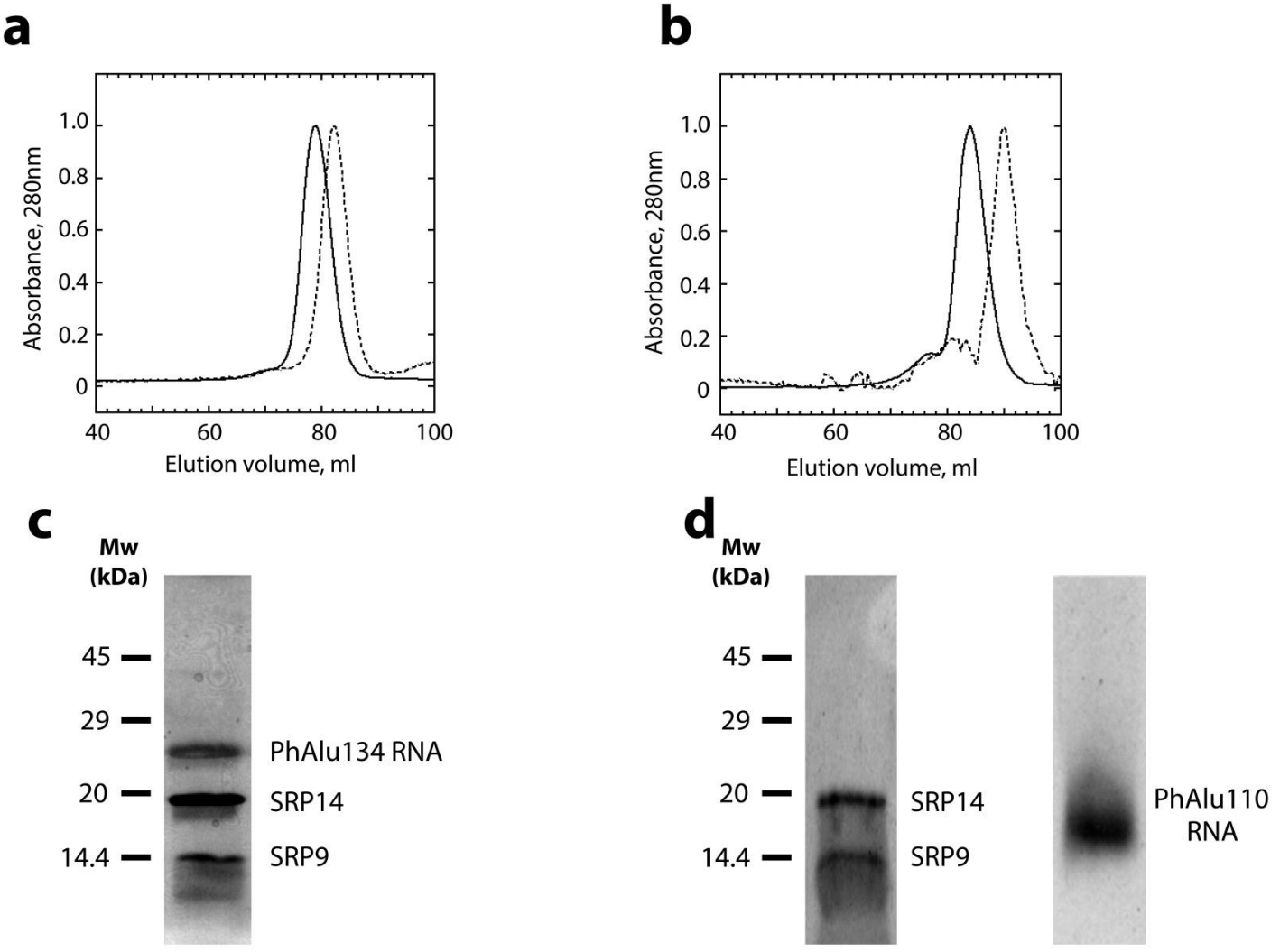

Supplementary Figure 2

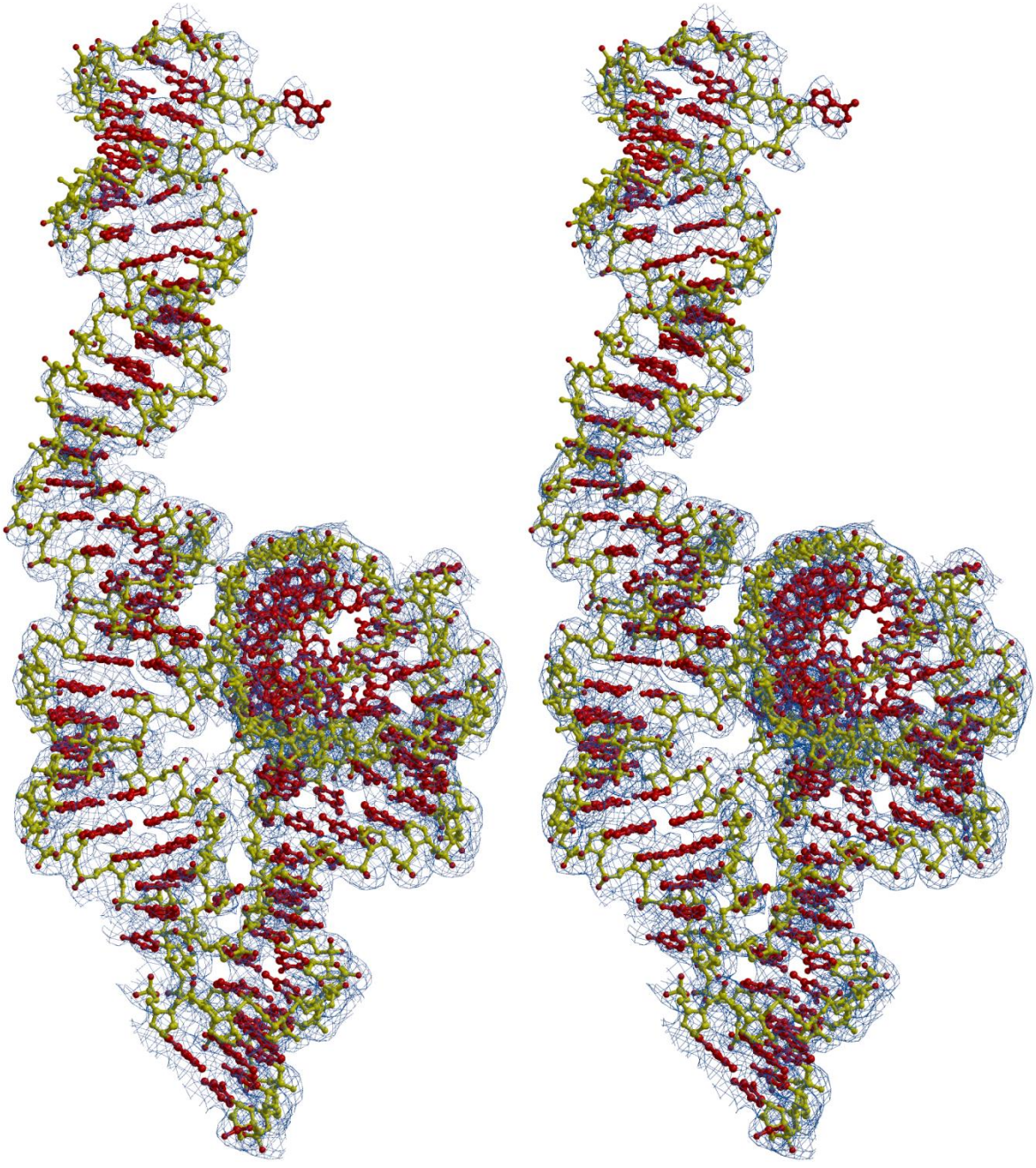

Supplementary Figure 3

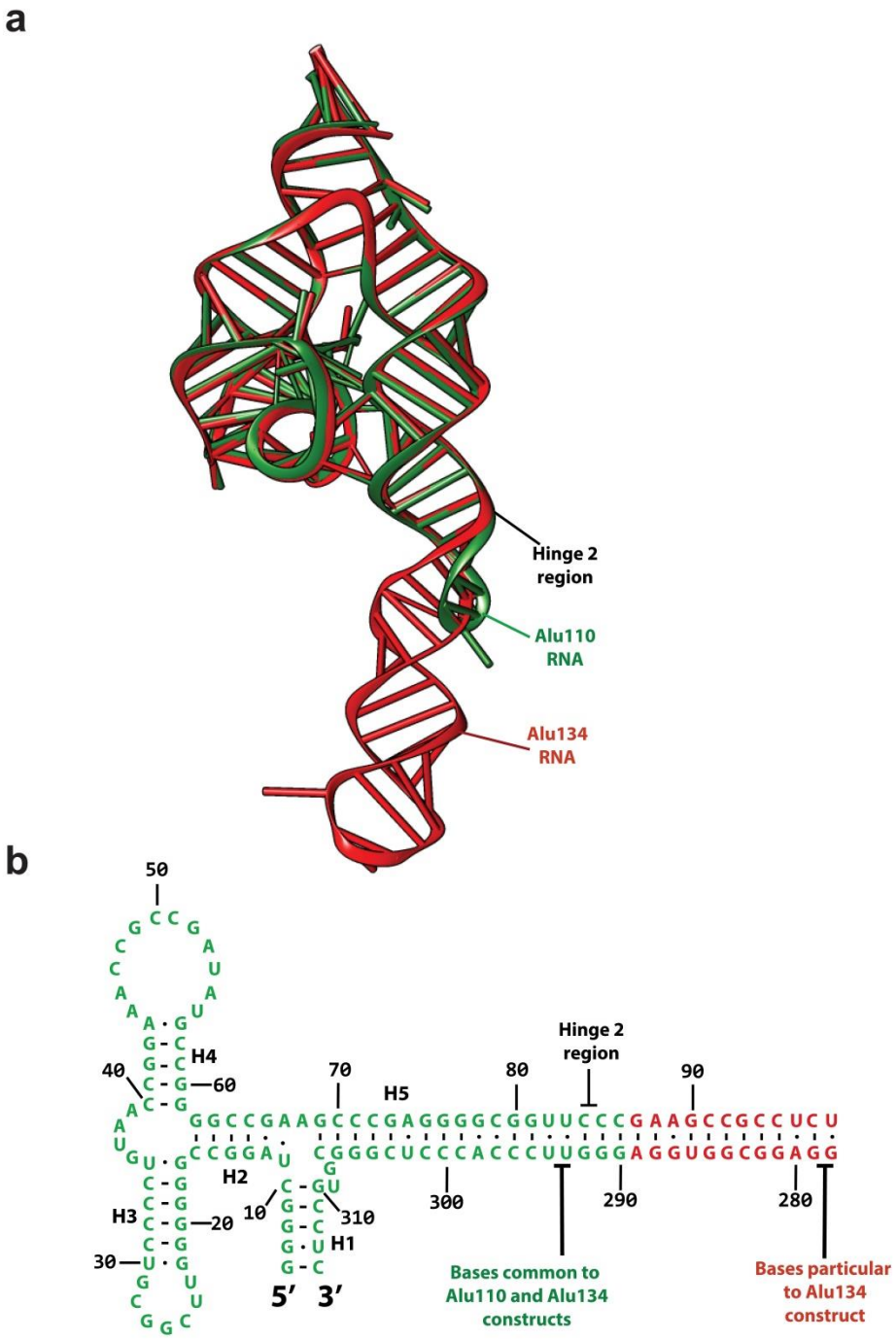

Supplementary Figure 4